Influence of Central Siberian snow-albedo feedback on the spring East Asian dust cycle and connection with the preceding winter Arctic oscillation

Journal of Geophysical Research: Atmospheres

RESEARCH ARTICLE
10.1029/2018JD029385

Influence of Central Siberian Snow-Albedo Feedback on the Spring East Asian Dust Cycle and Connection With the Preceding Winter Arctic Oscillation

Heng Liu[1,2], **Xiaodong Liu**[1,2,3], **and Buwen Dong**[4]

[1]SKLLQG, Institute of Earth Environment, Chinese Academy of Sciences, Xi'an, China, [2]College of Earth and Planetary Sciences, University of Chinese Academy of Sciences, Beijing, China, [3]CAS Center for Excellence in Tibetan Plateau Earth Sciences, Beijing, China, [4]National Centre for Atmospheric Science, University of Reading, Reading, UK

Key Points:
- The enhanced East Asian dust emission is associated with a cyclonic wind anomaly induced by Central Siberian mid-lower troposphere cooling
- The Central Siberian cooling is attributed to local snow-albedo and cloud-albedo feedbacks
- Winter Arctic Oscillation leads to changes in surface temperature in Siberia and induces positive snow-albedo and cloud feedbacks in spring

Supporting Information:
- Supporting Information S1

Correspondence to:
X. Liu,
liuxd@loess.llqg.ac.cn

Citation:
Liu, H., Liu, X., & Dong, B. (2018). Influence of Central Siberian snow-albedo feedback on the spring East Asian dust cycle and connection with the preceding winter Arctic Oscillation. *Journal of Geophysical Research: Atmospheres*, *123*. https://doi.org/10.1029/2018JD029385

Received 10 MAR 2018
Accepted 15 NOV 2018
Accepted article online 29 NOV 2018

Abstract The Asian dust cycle has significant effects on the climate and environment, while its spatiotemporal variability and change mechanisms are not yet completely understood. Reanalysis data from the Modern-Era Retrospective Analysis for Research and Applications, version 2 (MERRA2), data set are used to explore the spatiotemporal distribution of the East Asian dust cycle and possible reasons for the interannual variations. Based on the empirical orthogonal function analysis, the dominant mode of dust emissions from the East Asian deserts in the dust season (spring) shows that the Gobi Desert contributes most of the interannual variance of dust emissions in East Asia. The patterns of the regional circulation, temperature, and radiation are analyzed by regressing these variables against the principal component time series of the first empirical orthogonal function mode. The results show that the enhanced dust emissions are associated with a cyclonic circulation anomaly and cooling in the lower and middle troposphere over Central Siberia. The cooling is attributed to local snow-albedo and cloud-albedo feedbacks. The surface cooling is conducive to maintain the snow cover, whereas the cooling in the middle troposphere is associated with the increase of the relative humidity and cloud cover. The increased snow and cloud cover reflect more shortwave radiation, tending to maintain or amplify the surface cooling. It is also found that the negative phase of the Arctic Oscillation in winter initiates the surface cooling in the next spring and results in positive snow-albedo and cloud feedbacks in Central Siberia, eventually enhancing the East Asian dust cycle.

1. Introduction

Mineral dust aerosols, which are mainly emitted from arid and semiarid areas, have an important role in the Earth's radiation budget, climate dynamics, cloud microphysics, and the maritime carbon cycle (Knippertz & Stuut, 2014). Atmospheric dust loading significantly affects the Earth's radiation budget (Miller & Tegen, 1998; Sokolik & Toon, 1996; Tegen et al., 1997). The energetics of the atmosphere, including easterly waves and the development of tropical cyclones over the Atlantic Ocean, are modified by the radiative heating of dust (Karyampudi & Carlson, 1988; Karyampudi & Pierce, 2002). Levin et al. (1996) observed that desert dust particles coated with sulfate form large and effective cloud condensation nuclei. As atmospheric dust can be transported for thousands of kilometers, it is also a source of micronutrients that can fertilize continental and marine ecosystems far from its source regions (Bishop et al., 2002; Bristow et al., 2010; Falkowski et al., 1998; Mahowald et al., 2005).

The interior of East Asia is a major source of airborne dust (Prospero et al., 2002; Rea, 1994; Rea & Hovan,1995; Su & Fung, 2015; Washington et al., 2003). Deserts are found from the Tarim Basin to the border between northern China and Mongolia (Figure 1; Deer, 1984; Liu et al., 2004; Merrill et al., 1989, 1994; Zhang et al., 1997, 2003). The Asian dust cycle is mainly active in spring, and there is a high frequency of dust storms (Liu et al., 2004). The East Asian dust storms can impact the aerosol particle number concentration and size distribution (Manktelow et al., 2010), shortwave radiation directly and indirectly (Huang et al., 2014), cloud, and precipitation (Kawamoto, 2008; Yin & Chen, 2007) and finally influence the climate and weather in the source and downstream areas. So it is important to have a better understanding of East Asian dust emission and cycling process. Some researchers have studied the East Asian dust cycle to determine the characteristics of the emission, transportation, and sedimentation of dust by using limited observational data. For example, by analyzing observational data from meteorological stations between 1960 and 1999, Sun et al. (2001) found that the main source areas of dust storms in northern China were located in the Gobi and Taklimakan Deserts

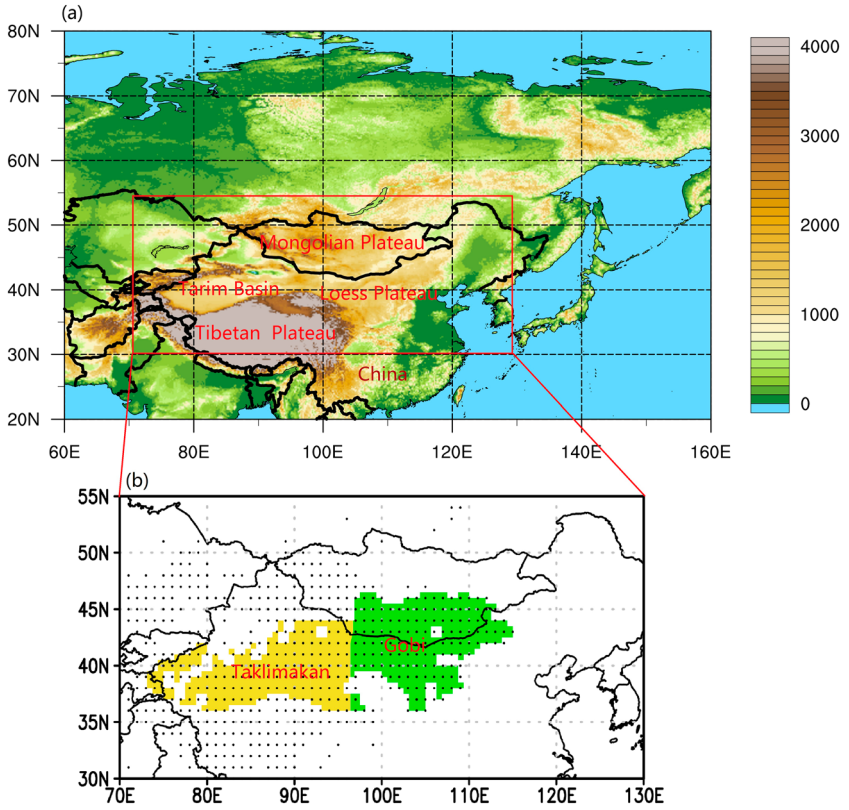

Figure 1. (a) Topographic distribution of East Asia and (b) locations of main deserts of the study area. Colored areas in (a) represent altitude (m). The green and yellow colored areas in (b) indicate the Gobi Desert and Taklimakan Desert, respectively. Dotted areas represent those with an annual mean normalized difference vegetation index less than 0.2 and the grids with higher than 10^{-12} kg·m^{-2}·s^{-1} dust emission flux in Modern-Era Retrospective Analysis for Research and Applications, version 2 (MERRA2), are determined as deserts.

and that the high frequency of dust storms in the 1970s was related to drought conditions in these deserts. Wang et al. (2005) further investigated the spatial distribution of dust storm, blowing dust, and floating dust weather. Sun et al. (2005) analyzed the chemical composition of dusts and found that the dust storms observed in Beijing in 2002 mainly originated from the central and western deserts of Inner Mongolia, the Loess Plateau, and the Gobi Desert. By investigating the first full year of Cloud-Aerosol Lidar and Infrared Pathfinder Satellite Observation (CALIPSO) measurements, Liu, Liu, et al. (2008) found numerous large dust plumes over the northern slopes and eastern Tibetan Plateau in spring 2007, with source regions located to the north and on the eastern part of the plateau.

Previous studies on the East Asian dust cycle are mainly focused on the variations and their mechanisms in the Asian dust storm frequency (DSF). Littmann (1991) calculated the correlation between the time series of the DSF and climatic parameters and found that the Asian DSF was related to precipitation and wind speed. Liu et al. (2004) found that the link between antecedent precipitation and the subsequent DSF was the soil moisture content and its persistence. Ding et al. (2005) showed that the spring cyclonic circulation anomaly over the Mongolian Plateau and Central Siberia affected the DSF in northern China. The East Asian dust cycle responds not only to the influence of regional circulation and land surface conditions but also to large-scale teleconnections. For example, the Arctic Oscillation (AO), the dominant mode of large-scale atmospheric circulation variability between the middle and high latitudes of the Northern Hemisphere, has a significant correlation with the DSF on the decadal scale (Gao & Washington, 2010; Mao et al., 2011). Due to the lack of observational data, relevant studies only discussed the statistical correlation of AO with Asian DSF from the surface observation (Gong et al., 2006; Han et al., 2008) or the aerosol optical depth (AOD) retrieved from satellites (Gao & Washington, 2010). Thus, our understanding of the spatiotemporal distribution of Asian dust emission, transportation, and sedimentation is still limited. The

mechanism of the linkage between the East Asian dust cycle and the large-scale circulation is also not fully understood. In this study, we use newly released dust-related reanalysis data from the National Aeronautical and Space Administration to further determine the relationship of Asian dust cycle interannual variability with the regional and large-scale background circulations and its underlying mechanism. The data and methodologies are described in section 2. Section 3 describes characteristics of the East Asian dust cycle, the related regional circulation pattern, and the possible snow-albedo and cloud feedback processes. How the AO initiates the snow-albedo and cloud feedbacks is also discussed in section 3. Section 4 is a discussion and summary of our results.

2. Data and Methods

The dust-related variables were mainly acquired from newly released reanalysis data from the Modern-Era Retrospective Analysis for Research and Applications, version 2 (MERRA2), data set (Gelaro et al., 2017) produced by the National Aeronautical and Space Administration's Global Modeling and Assimilation Office. The data set assimilates data for the AOD from various ground- and space-based remote sensing platforms (Randles et al., 2017). In the assimilation system, potential dust sources are determined based on the observed correlation of dust-emitting regions with large-scale topographic depressions (Ginoux et al., 2001). The dust have wind-speed-dependent emissions (Randles et al., 2017). For each size bin, the dust parameterization developed by Marticorena and Bergametti (1995) is applied. MERRA2 supplies various variables describing a complete dust cycle composed of dust emission, transportation, and sedimentation in five bins. These variables include the 1980–2016 hourly to monthly mean dust emission flux, the dust column mass density, the dust surface mass concentration, the dust column horizontal mass flux, and the dust sedimentation flux at a spatial resolution of longitude 0.625° × latitude 0.5°. This makes it possible to determine variations in the East Asian dust cycle on different timescales based on emissions from deserts (Buchard et al., 2017). Meanwhile, we used the 2007–2016 monthly AOD data from CALIPSO with a spatial resolution of longitude 5° × latitude 2°, 2000–2016 monthly AOD data from Multi-angle Imaging SpectroRadiometer (MISR) MIL3MAE (https://misr.jpl.nasa.gov/) with a spatial resolution of 0.5° × 0.5°, and 2002–2017 monthly AOD data from Moderate Resolution Imaging Spectroradiometer (MODIS) MYD08 (https://modis.gsfc.nasa.gov/) with a spatial resolution of 1° × 1° to describe the spatial distribution of dust loading (Liu, Liu, et al., 2008; Winker et al., 2006, 2007) for comparison with the MERRA2 data set. In addition, the Chinese DSF calculated from hierarchical dust storms based on data from 442 meteorological stations in northern China were used to describe the intensity of the dust cycles (Kang et al., 2016; Wang et al., 2008). The dust weather records of meteorological stations were supplied by the National Meteorological Information Center of the China Meteorological Administration (http://www.nmic.gov.cn/). Considering of the intensity of dust storm weather divided as floating dust (*F*), blowing dust (*B*), and dust storm (*S*), the integrated DSF for a specific time period at any station can be calculated as follows:

$$DSF = 9\times S + 3\times B + F$$

Meteorological parameters were obtained from both the MERRA2 and European Centre for Medium-Range Weather Forecasts (ECMWF) Re-Analysis (ERA)-Interim data sets (Dee et al., 2011). The 1980–2016 winter and spring 700-hPa winds, 500-hPa geopotential height, temperature of land surface, soil temperature, surface air temperature, and 1,000- to 200-hPa vertically resolved temperature fields at a horizontal resolution of longitude 0.625° × latitude 0.5° were extracted from the MERRA2 data set to explore their relation to the Asian dust cycles. The same parameters for the same time periods from the independent ERA-Interim data set with a spatial resolution of 0.5° × 0.5° were employed in the supporting information to compare with the MERRA2 data set. The 1980–2016 spring snow cover, surface albedo, total cloud area fraction, snowfall, surface incoming shortwave flux, surface net downward shortwave flux, surface net downward longwave flux, and other related radiative variables with a spatial resolution of longitude 0.625° × latitude 0.5° from the MERRA2 data set were used to analyze the snow-albedo feedback. The 1980–2016 monthly AO indices were obtained from the National Oceanic and Atmospheric Administration Climate Prediction Center (http://www.cpc.noaa.gov/products/precip/CWlink/daily_ao_index/ao_index.html). AO is a large-scale natural mode of atmospheric circulation variability that exists in the Northern Hemisphere from the surface to the stratosphere, and the monthly index is defined as the empirical orthogonal function (EOF) first-mode time series of the Northern Hemisphere (poleward of 20°N) sea-level pressure (Thompson et al., 2000).

Snow cover data and the normalized difference vegetation index were applied in this research. The 1980–2016 weekly values of the snow cover extent that shows the fraction of snow cover from 1979 to 2014 with 88 grid cells over the Northern Hemisphere were obtained from the National Oceanic and Atmospheric Administration snow chart climate data record (Brown & Robinson, 2011) archived at Rutgers University (http://climate.rutgers.edu/snowcover/) and then were interpolated and compared with the albedo in the MERRA2 data set. This data set has been used previously to investigate the role of snow cover in the climate system and is considered to be a reliable data set for conducting climate-related studies (Brown, 2000; Brown et al., 2010). The 2000–2015 monthly mean normalized difference vegetation index was acquired from the MODIS vegetation index (MOD13; Huete et al., 2002; Miura et al., 2001) and then interpolated into longitude 0.625° × latitude 0.5° to distinguish the desert lands.

The EOF analysis method (Björnsson & Venegas, 1997) was applied to decompose the modes of dust emission interannual variability in spring (March–April–May) average during the period of 1980–2016 (37 years) in East Asian deserts (total 1,008 grids shown in Figure 1b). Linear regression (Wang & Zhang, 2015) was applied to reveal the corresponding circulation, temperature, radiation, and dust patterns with respect to the time series of the first EOF mode of East Asian dust emission variability. We also tried to explore possible cause-effect relations among different variables by calculating lead-lag correlation coefficients (Liu et al., 2017; Wang & Zhang, 2015) of hourly Siberian surface air temperature and shortwave radiation with 700 hPa and surface winds over deserts and dust emission in the spring of 2010. Additionally, the method of general equilibrium feedback assessment (Liu, Wen, et al., 2008; Yu et al., 2017a, 2017b) was applied to reveal the effect of snow-albedo feedback and cloud-albedo feedback on Central Siberian spring surface air temperature.

3. Results

3.1. Spatiotemporal Distribution of the Climatological East Asian Dust Cycle

Dust emission is a starting point of the dust cycle. The spatial distributions of the multiyear mean AOD obtained from MISR (Figure 2a) and MODIS (Figure 2b) show the high-value areas consistent with those of the strong dust emission in the Taklimakan Desert located in the Tarim Basin (80–98°E) and the Gobi Desert located on the border of China and Mongolia (98–110°E; Figure 2c) where human activities are relatively low. The annual emissions of PM_{10} dust (the sum of five bins) from the Taklimakan and Gobi Deserts are 59 and 32 Tg, respectively. Xuan and Sokolik (2002) estimated that the Taklimakan Desert contributes 64% of the emission in China, while the Gobi Desert contributes 35%. The emission of dust is the key factor determining the distribution of airborne dust. The standardized multiyear mean annual cycles of dust emission from the Gobi Desert and the Taklimakan Desert (colored in Figure 1b), AOD over the desert region (70–110°E, 35–45°N), and DSF of northern China (Figure 2d) all show peaks in spring, suggesting that a stronger emission of dust from East Asian deserts leads to a higher dust loading in the atmosphere in the source area and a more frequent DSF in northern China during the dust season, as reported previously by Sun et al. (2001), Liu et al. (2004), and Wang et al. (2005). These comparisons confirm the reliability of the MERRA2-obtained dust data. In the following, therefore, we mainly focus on boreal spring and use the spring dust and meteorological data from the MERRA2 data set to explore the dust-circulation linkage.

The climatological spring mean airborne East Asian dust density and sedimentation flux are well matched with the dust emission. As shown in Figure 3a, the spatial distribution of the spring mean dust column mass indicates that airborne dust over East Asia is mainly concentrated in the Taklimakan and Gobi desert regions. The density of airborne dust gradually decreases from west to east and reaches 700 mg/m^2 over the Taklimakan Desert, 200 mg/m^2 over the Gobi Desert, 100 mg/m^2 from eastern China to southwestern Japan, and 70 mg/m^2 over the western North Pacific. The distribution of dust surface mass is restricted in northern and eastern China, although it also decreases from west to east (Figure 3b), reaching concentrations of 0.4 mg/m^3 over the Taklimakan Desert, 0.1 mg/m^3 over the Gobi Desert, 0.02 mg/m^3 over northeastern China, and 0.01 mg/m^3 over the Korean Peninsula and surrounding areas. The surrounding areas of desert and northern China, with a higher dust surface mass concentration, are also occasionally affected by dust storms. The distribution of dust sedimentation flux resembles that of dust surface mass concentration (Figure 3c). The sedimentation flux reaches 100 $mg{\cdot}m^{-2}{\cdot}day^{-1}$ over the Taklimakan Desert, 20 $mg{\cdot}m^{-2}{\cdot}day^{-1}$ over the Gobi Desert, 4 $mg{\cdot}m^{-2}{\cdot}day^{-1}$ over northeastern China, 2 $mg{\cdot}m^{-2}{\cdot}day^{-1}$ over the Korean Peninsula,

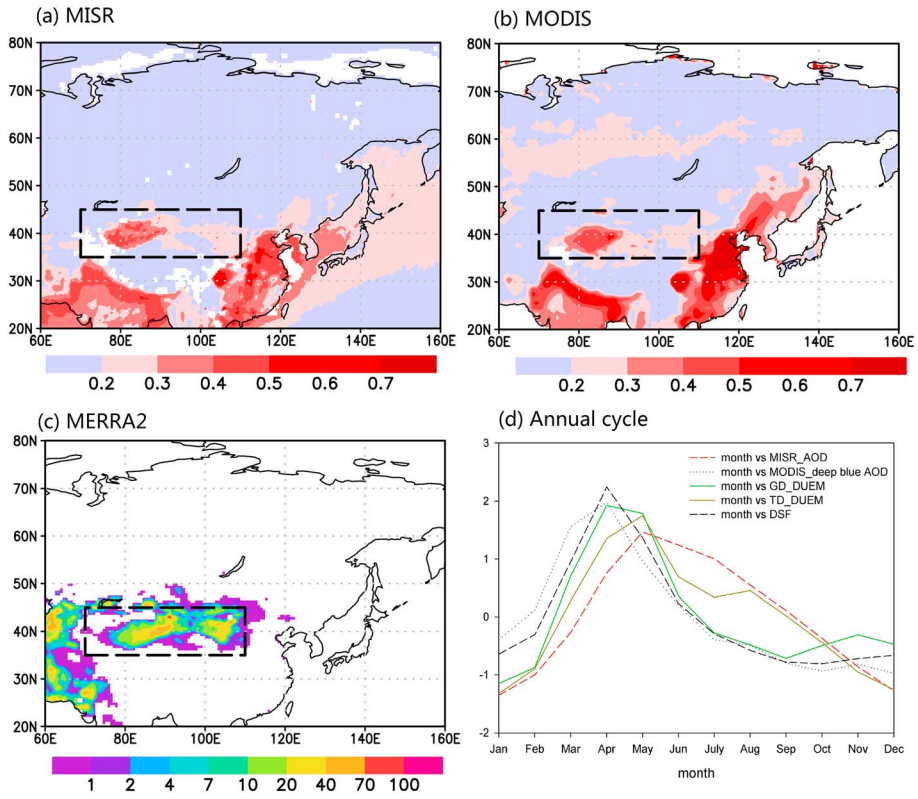

Figure 2. Distributions of the climatological (a) annual mean aerosol optical depth (AOD; colored) from 2000 to 2016 in Multi-angle Imaging SpectroRadiometer (MISR) and (b) annual mean AOD from 2002 to 2017 (colored) in Moderate Resolution Imaging Spectroradiometer (MODIS). (c) The annual mean dust emission (colored, unit: $mg{\cdot}m^{-2}{\cdot}day^{-1}$) in the Modern-Era Retrospective Analysis for Research and Applications, version 2 (MERRA2), data set from 1980 to 2016. (d) Standardized multiyear mean annual cycles of dust emission from East Asian deserts in the MERRA2 data set (solid lines), the AOD averaged for the desert region (70–110°E, 35–45°N) in the MISR and MODIS data sets (dashed lines), and the dust storm frequency (DSF) in northern China (dot line). The black dashed line boxes in (a), (b), and (c) represent the desert region of East Asia.

and 1 $mg{\cdot}m^{-2}{\cdot}day^{-1}$ over the western North Pacific. The interannual variation of MERRA2 surface mass concentration is highly and positively correlated with that of the DSF of meteorological stations (more than 100 stations) in or near the deserts (Figure 3d), indicating close correspondence between dust surface concentration and DSF. That means the spatial distributions of dust surface concentration in the MERRA2 data set agree with the ones of DSF discovered by Wang et al. (2005).

The characteristics of the spring circulation were studied in an attempt to understand the climatological background of the distribution of East Asian dust. As illustrated in Figure 4a, the East Asian deserts and downstream areas are mainly controlled by northwesterly winds in spring. The surface temperature in East Asia decreases from south to north. The distributions of the 700-hPa circulation and surface air temperature for the same period in the ERA-Interim data set are in agreement with Figure 4a (see the supporting information). According to the principle of thermal winds, the increase in the temperature gradient between Mongolia and northern China benefits northwesterly winds over the East Asian deserts in spring and the strengthened winds is closely related to the higher DSF in northern China as suggested by Qian and Zhu (2001). The spatial variations of the spring mean dust column mass transportation and dust emission follow the northwesterly winds (Figure 4b). East Asian dust is mainly transported from the source regions to the east. The average transportation flux reaches 4 $g{\cdot}m^{-1}{\cdot}s^{-1}$ over northern China. In spring, when the northwesterly winds over East Asian deserts exceed a threshold velocity, the surface dust can be mobilized locally, uplifted, and transported eastward to eastern China and even remote Pacific Ocean (Randles et al., 2017). Thus, the northwesterly winds are extremely effective in both the emission and transportation of dust.

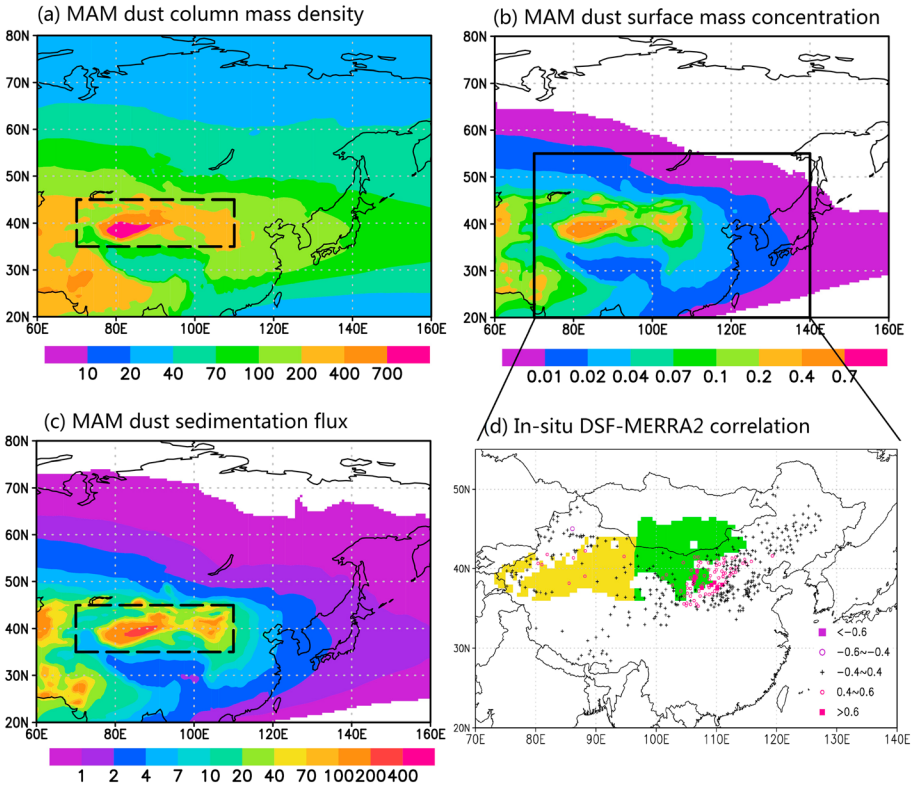

Figure 3. Distribution of the climatological spring (March–April–May [MAM]) mean (a) dust column mass density (mg/m^2), (b) dust surface mass concentration (mg/m^3), and (c) dust sedimentation (mg·m^{-2}·day^{-1}) in the Modern-Era Retrospective Analysis for Research and Applications, version 2 (MERRA2), data set during 1980–2016. (d) Distribution of correlation coefficients between spring dust surface concentration interannual variability in MERRA2 and spring dust storm frequency (DSF) interannual variability at 442 stations in northern China during 1980–2013. The black dashed line boxes represent the East Asian deserts. The green and yellow areas in (d) indicate the Gobi Desert and Taklimakan Desert, respectively.

3.2. Interannual Covariations of Spring East Asian Dust Emission and the Regional Circulation

EOF analysis was applied to determine the interannual variations in the spatiotemporal characteristics of spring dust emissions from East Asian deserts during 1980 to 2016. The first EOF mode, explaining 30.50% of the total variance, shows consistent positive anomalies in dust emissions from East Asian deserts with large values over the Gobi Desert (Figure 5a). The time series of the first mode is well matched with the time

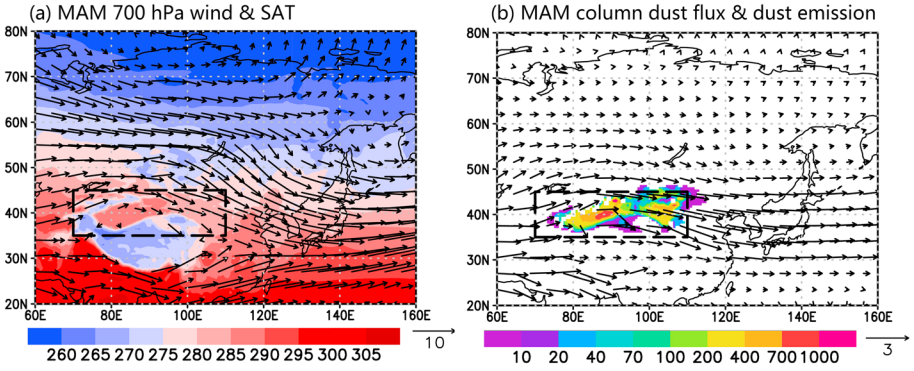

Figure 4. (a) Climatological spring (March–April–May [MAM]) mean 700-hPa wind (vectors, unit: m/s) and surface air temperature (SAT; colored, unit: K) fields in the Modern-Era Retrospective Analysis for Research and Applications, version 2 (MERRA2), data set. (b) Climatological spring mean horizontal transport flux of column dust load (vectors, unit: g·m^{-1}·s^{-1}) and surface dust emission flux (colored, unit: mg·m^{-2}·day^{-1}) in East Asian deserts in the MERRA2 data set. The black dashed line boxes represent the East Asian desert regions.

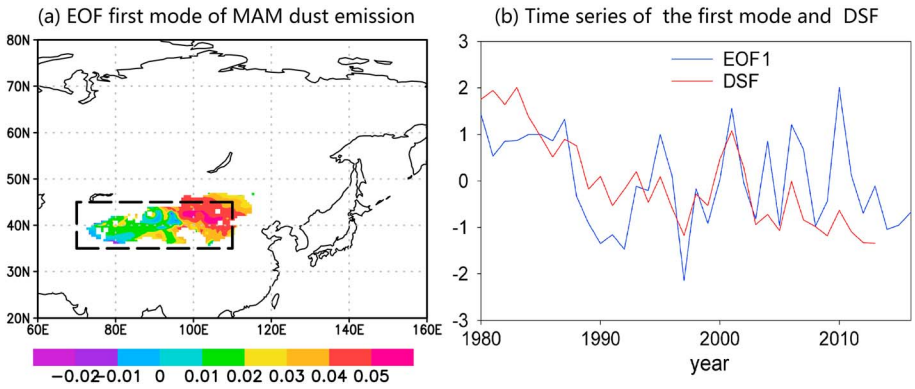

Figure 5. (a) Spatial pattern of the first empirical orthogonal function (EOF) mode of spring mean dust emission flux in East Asian deserts during 1980–2016 based on the Modern-Era Retrospective Analysis for Research and Applications, version 2 (MERRA2) data set. (b) Time series of the first EOF mode and standardized year-to-year variation of the spring East Asian dust storm frequency (DSF) calculated based on 442 Chinese meteorological stations. The black dashed line box in a represents the East Asian desert region. MAM = March–April–May.

evolution of mean DSF in northern China, with a correlation coefficient of 0.56, passing Pearson's correlation test at the 99% significance level (Figure 5b). The time series of the first EOF has a strong interannual variation and the same decreasing trend as the DSF. There is a high value period during 1980–1986, which has been reported previously by Ding et al. (2005). These results indicate a close relationship between dust emission and DSF interannual variations and suggest that the time series of the dominant mode of dust emissions from East Asian deserts is therefore a suitable proxy for the main mode of the interannual variations of the East Asian dust cycle.

To determine the circulation pattern influencing the interannual variability of dust emission, the spring mean circulation in the MERRA2 data set was regressed against the time series of the first EOF mode. The results show that negative 500-hPa geopotential height regression coefficients, a cyclonic circulation anomaly over Central Siberia, and anomalous northwesterly winds at 700 hPa over East Asian deserts are associated with the positive phase of the dust emission mode (Figure 6a), indicating increased spring northwesterly winds over East Asian deserts in years with high dust emission. These results are in line with Ding et al. (2005) who showed anticyclonic circulation anomalies over the Central Siberia-Mongolia Plateau were accompanied with decadal decrease in dust storm activity from the 1980s to the 1990s (red line in Figure 5b). Significant negative surface air temperature regression coefficients are also detected over Central Siberia (Figure 6b). The temperature and geopotential height regression coefficients are centered near Lake Baikal. The negative temperature regression coefficients more than 1 °C are likely responsible for the formation of the cyclonic circulation anomaly in the lower troposphere (Figure 6a). The longitude-pressure cross-section of temperature and the geopotential regression coefficients map along 55°N (Figure 6c), where the center of the cyclonic anomaly is located, give the answer. Significant negative temperature regression coefficients are in the lower and middle troposphere, and a positive temperature regression coefficients are in the upper troposphere from 80°E to 140°E (Figure 6c). This change in temperature regression coefficients with height means higher air density below 300 hPa and lower density in the upper troposphere. Therefore, the height of the isobaric surface decreases in the lower troposphere and the center of height regression coefficients locate at 300 hPa where temperature regression coefficients change sign. It is therefore the cooling at the surface and lower troposphere that promotes the development of a midlatitude trough in the middle and lower troposphere. In addition, the relative large cooling in Central Siberia in the lower troposphere leads to a greater temperature gradient between the north and south sides of the deserts, and this enhances northwesterly winds according to thermal wind balance. Thus, the variations in temperature in the middle and lower troposphere over Central Siberia result in the regional cyclonic anomalies and anomalous northwesterly winds on East Asian deserts, especially with large anomalies over the Gobi Desert. From the cross-section of the climatological spring average wind vectors along 40°N (Figure 6e), it can be seen that the Taklimakan Desert surrounded by mountains is controlled by easterly winds at the surface, while the Gobi Desert on Mongolian Plateau is controlled by westerly winds, although westerly winds prevail above 600 hPa over the two

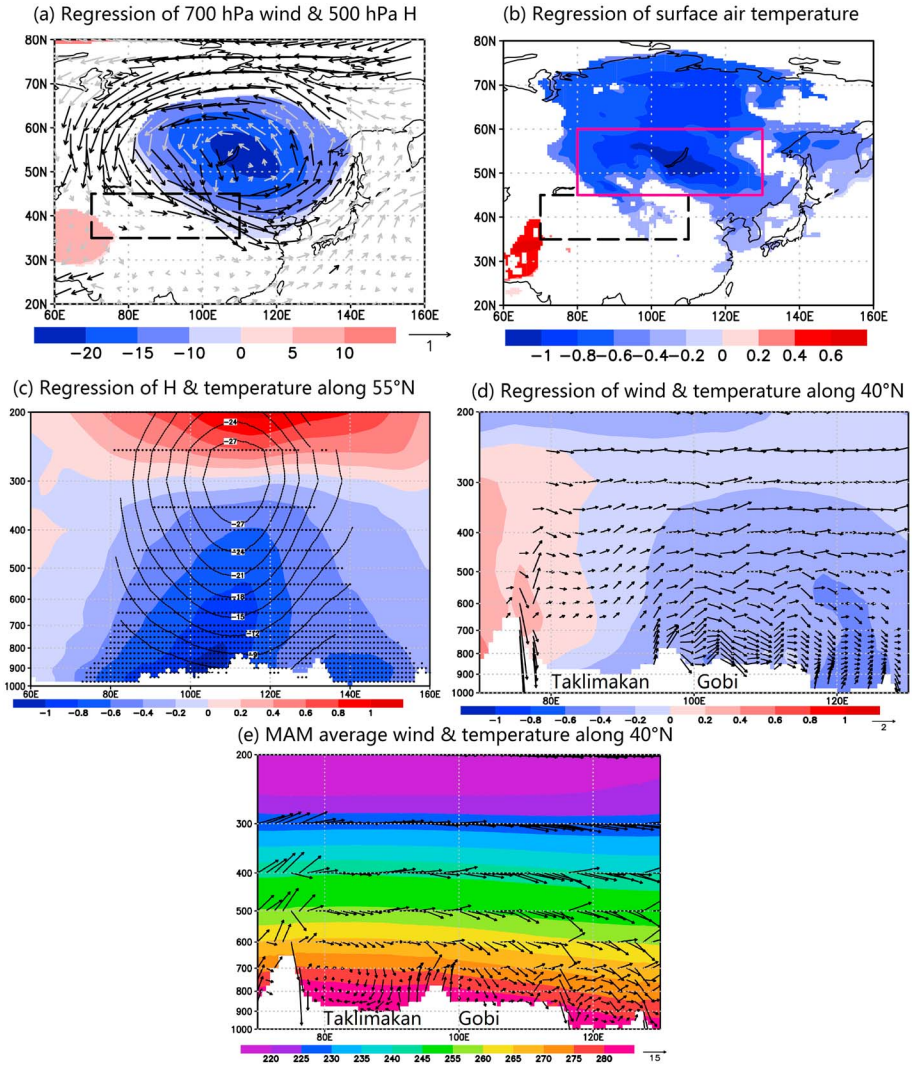

Figure 6. Spatial distributions of various variables in spring season (March–April–May [MAM]) linearly regressed against the time series of the first empirical orthogonal function (EOF) mode of the spring dust emission from East Asia deserts during 1980–2016. (a) 700-hPa wind (vectors, unit: m/s) and 500-hPa geopotential height (colored, unit: m) fields. (b) Surface air temperature (unit: K) in the Modern-Era Retrospective Analysis for Research and Applications, version 2 (MERRA2), data set. (c) Longitude-pressure cross-section of air temperature (colored, unit: K) and geopotential height (contours, unit: m) along 55°N. (d) Longitude-pressure cross-section of wind vectors (horizontal unit: m/s, vertical unit: -10^{-2} Pa/s) and air temperature (colored, unit: K) over the desert regions along 40°N. (e) The same as (d) but for the spring climatological mean. Colored areas in (a) and (b), black vectors in (a) and (d), and dotted areas in (c) pass the significance test at the 95% confidence level. The black dashed line boxes in (a) and (b) represent the East Asian desert regions. The red box in (b) indicates Central Siberia.

deserts. Regression analysis indicates that the upper-level wind speed over both the deserts and the surface westerly winds over the Gobi Desert are increased with the strengthening of dust emission, while the winds below 700 hPa over the Taklimakan Desert are not evidently changed (Figure 6d). The northwesterly thermal wind anomaly in the lower troposphere induced by the cooling over Central Siberia can surge into the surface of the Gobi Desert through the vertical exchange of the horizontal momentum induced by turbulent mixing (e.g., Wu et al., 2017). However, the vertical exchange of the horizontal momentum is weak over the Taklimakan Desert due to less lower tropospheric wind anomaly there and the blocking of the Tianshan mountain on the north border of the Desert.

To further demonstrate that the temperature anomaly over Central Siberia was directly associated with the dust activity over East Asian desert regions and interpret the mechanism, we took the spring of 2010 as an

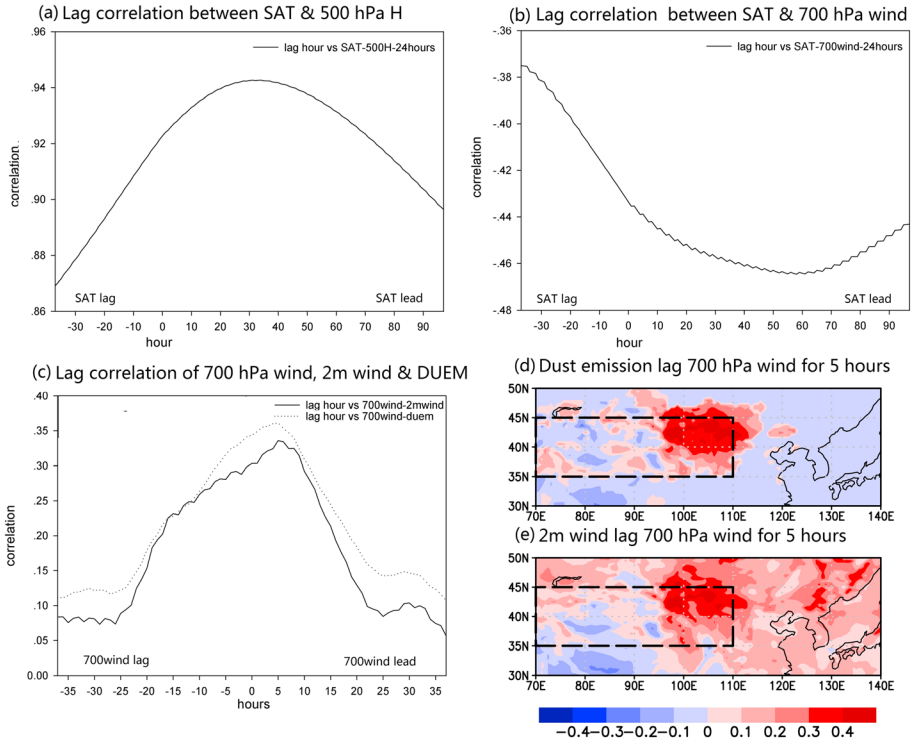

Figure 7. (a) Hourly lag correlations between the surface air temperature (SAT) and 500-hPa height averaged for Central Siberia (80–130°E, 45–60°N) in spring of 2010 with positive (negative) hours in the *x*-axis indicating SAT leading (lagging) 500-hPa height. (b) Hourly lag correlations between SAT averaged for Central Siberia and 700-hPa wind speed averaged for the Gobi Desert in spring of 2010 with positive (negative) hours in the *x*-axis indicating SAT leading (lagging) 700-hPa wind speed. (c) Hourly lag correlations of 700-hPa wind against 2-m wind speed and dust emission averaged for the Gobi Desert in March–April–May 2010 with positive (negative) hours in the *x*-axis indicating 700-hPa wind speed leading (lagging) 2-m wind speed and dust emission. (d) Correlation distribution between 700-hPa wind speed and 5-hr-lagged 2-m wind speed in spring of 2010. (e) The same as (d) but for 5-hr-lagged dust emission. Black boxes represent the East Asian desert regions. All hourly data are smoothed using 24-hr moving average.

example and choose hourly data to study lead-lag correlations between different variables. These lead-lag correlations indicate that the surface air temperature averaged for Central Siberia (80–130°E, 45–60°N) leads the 500-hPa height averaged for Central Siberia (80–130°E, 45–60°N) for about 30 hr (Figure 7a) and leads the 700-hPa wind speed averaged for the desert regions (90–110°E, 40–45°N) for about 60 hr (Figure 7b), while the 700-hPa wind speed leads the 2-m wind speed and dust emission for about 5 hr (Figure 7c) in the spring of 2010. The spatial distribution of the 5-hr lag correlations shows that the high-correlation centers are just located in the Gobi Desert (Figures 7d and 7e). These results indicate that the increase of 700-hPa wind has greater influences on the surface wind and then on dust emission over the Gobi Desert than the Taklimakan Desert.

It has been demonstrated in the previous sections that the spring surface temperature over Central Siberia is instrumental for the dust cycle variation over East Asia deserts. What factors are responsible for the surface temperature variation in spring? This question is addressed by analyzing the regional surface energy budget. The albedo, snow mass, and longwave and shortwave radiation were regressed against the first EOF mode time series of dust emission from 1980 to 2016, and regression results are shown in Figures 8 and 9. Corresponding to the strengthening of the spring dust emission in East Asia, the snow mass increases significantly in Central Siberia (45–60°N; Figure 8a), where the 500-hPa geopotential height anomalies are centered (Figure 6a). The satellite-retrieved spring snow cover extent (Figure 8c) and albedo (Figure 8b) and total cloud cover (Figure 8d) in MERRA2 also increase consistently in the same domain. It is possible that the increased spring snow mass leads to the increased surface albedo, which in turn leads to the reduced surface net downward shortwave radiation. The cross-section of the relative humidity regression along 55°N indicates an increase in the lower and middle troposphere (Figure 8e), corresponding to anomalous cold temperature

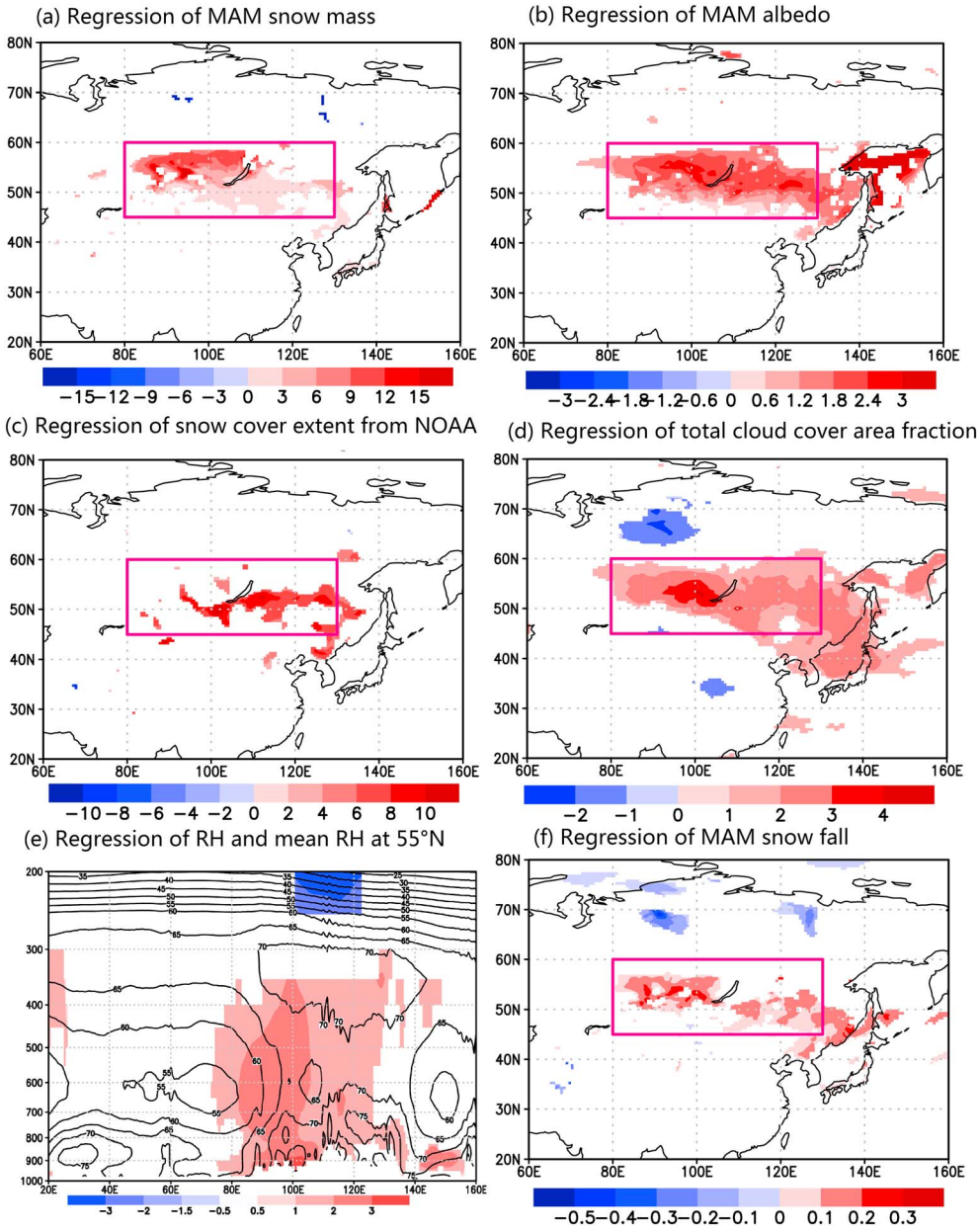

Figure 8. Regressions of spring (March–April–May [MAM]) seasonal mean (a) snow mass (unit: kg/m^2), (b) albedo (unit: %), (c) snow cover extent (unit: %), (d) total cloud area fraction (unit: %), (e) longitude-pressure cross section of relative humidity (RH; colored, unit: %; contours show the climatological RH) along 55°N, and (f) snowfall (unit: kg·m^{-2}·day^{-1}) against the time series of the empirical orthogonal function mode of dust emission. Snow cover extent is from the Global Snow Laboratory, Rutgers University, and other variables are from the Modern-Era Retrospective Analysis for Research and Applications, version 1 (MERRA1), data set. Red box represents Central Siberia. Colored areas indicate that regressions pass the significance test at the 95% level. NOAA = National Oceanic and Atmospheric Administration.

(Figure 6c). However, the specific humidity in the same region as in Figure 8e is not significantly changed (not shown). The cooling air temperature in the lower and middle troposphere facilitates the condensation of moisture, increases cloud cover (Figure 8d), and therefore increases snowfall (Figure 8f). The same regressions of low cloud cover and medium cloud cover in ERA-Interim show significant increases, too (see the supporting information). It is expected that the increase in the snow cover extent, snow mass, and the total cloud cover should lead to reducing the net surface downward shortwave radiation, which helps maintain the surface cooling.

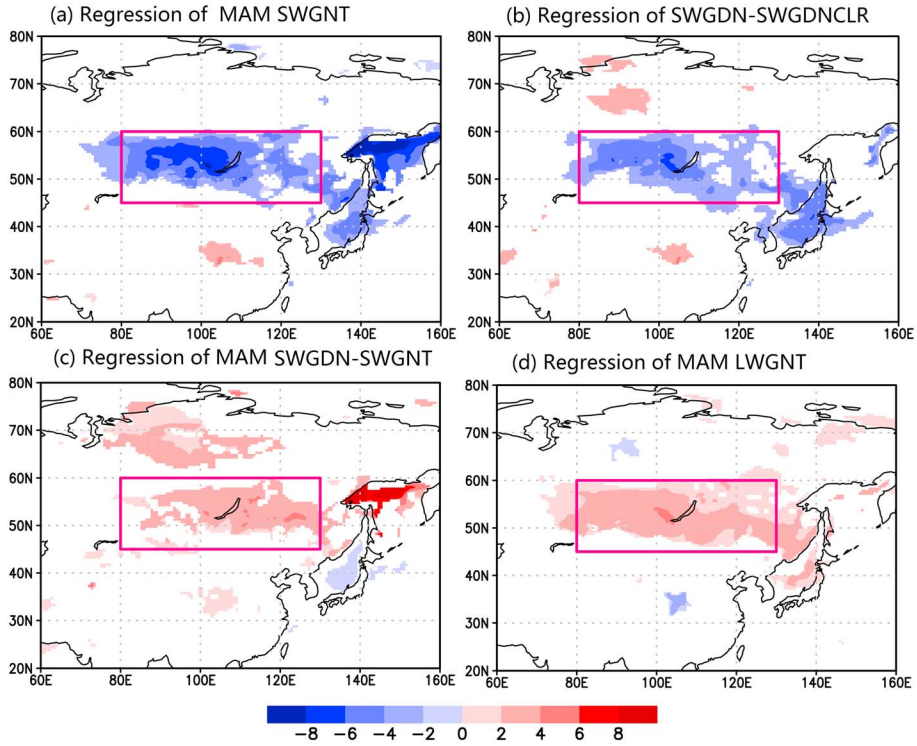

Figure 9. Regression maps of spring (March–April–May [MAM]) seasonal mean (a) surface net downward shortwave flux (SWGNT); (b) shortwave cloud radiative effect, the difference between surface incoming shortwave radiation flux (SWGDN) and surface incoming shortwave radiation flux without cloud (SWGDNCLR); (c) surface shortwave reflection (SWGDN-SWGNT); and (d) surface net upward longwave flux (LWGNT) in the Modern-Era Retrospective Analysis for Research and Applications, version 2 (MERRA2), data set (unit: W/m^2) against the time series of the empirical orthogonal function mode of dust emission. Red box represents Central Siberia. Colored areas indicate that regressions pass the significance test at the 95% level.

The regression map of surface net downward shortwave flux illustrates that during springs with high dust emission over East Asia, significant negative surface net downward shortwave flux regression coefficients of up to −6 W/m^2 occurred in Central Siberia (45–60°N; Figure 9a). This decrease in net shortwave radiation implies that more radiation is reflected by increased cloud cover (Figure 8d) and increased the Earth's surface albedo (Figure 8b). The regressed shortwave cloud radiative effect regression coefficients (difference between surface incoming shortwave flux and surface incoming shortwave flux without cloud) mainly occurred on the west of Baikal (Figure 9b). The differences in the regressed surface incoming shortwave flux and surface net downward shortwave flux (Figure 9c) represent the shortwave radiation reflected by the surface albedo. When more dust is emitted from the East Asian deserts (positive phase of dust emission EOF mode), the majority of the grids in the domain shows positive regression coefficients up to 2 W/m^2, indicating increased reflected upward shortwave flux by the surface (Figure 9c). At the same time, less longwave radiation is emitted upward in the domain (Figure 9d), reflecting reduced upward longwave flux from the cold surface in Central Siberia based on the equation for black body radiation. So the changes in snow albedo and cloud albedo play important roles in Central Siberian energy budget and lower-middle troposphere temperature variation.

Table 1 is a summary of the mean values, regression coefficients, and correlation coefficients for the area mean variables in Central Siberia. Both the surface albedo and total cloud cover over Central Siberia increase significantly during the years with high dust emission. The regression of the reflected shortwave radiation from the surface is 1.88 W/m^2, whereas that from the incoming surface shortwave is −1.64 W/m^2, resulted from increased total cloud cover. The regression of surface net downward longwave flux is 1.95 W/m^2, whereas the regression of the sensible heat flux from turbulence is up to −1.56 W/m^2, indicating reduced upward sensible flux. Therefore, the reduced net surface shortwave flux, through increased cloud cover

Table 1
Regressed Radiation-Related Variables in Central Siberia

Variable	Unit	Description	Mean	Regression coefficients	Correlation coefficient
albedo	%	Surface albedo	29.03	1.26	0.69**
cldtot	%	Total cloud area fraction	59.53	1.69	0.66**
H500	M	Height at 500 hPa	5448.83	−15.44	−0.69**
Hflux	W/ m^2	Sensible heat flux from turbulence	35.67	−1.56	−0.56**
lwgnt	W/m^2	Surface net downward longwave flux	−70.39	1.95	0.72**
precsno	kg·m^{-2}·day^{-1}	Snowfall	0.70	0.07	0.67**
prectot	kg·m^{-2}·day^{-1}	Total precipitation from atmospheric model physics	1.38	0.09	0.59**
snomas	kg/m^2	Total snow storage land	33.30	3.36	0.55**
swgdn	W/m^2	Surface incoming shortwave flux	202.44	−1.64	−0.56**
swgdnclr-swgdn	W/m^2	Reflected shortwave of cloud	61.78	2.95	0.69**
swgnt	W/m^2	Surface net downward shortwave flux	151.32	−3.52	−0.72**
swtnt	W/m^2	Total net downward shortwave flux	216.42	−3.62	−0.72**
swgdn-swgnt	W/m^2	Reflected shortwave of surface albedo	51.12	1.88	0.64**
Tlml	K	Surface air temperature	272.93	−0.75	−0.61**
tsurf_MAM	K	March–April–May surface temperature of land including snow	272.49	−0.92	−0.49**
tsurf_DJF	K	December–January–February surface temperature of land including snow	252.11	−0.84	−0.41*

*Significant at the 95% level. **Significant at the 99% level.

and increased surface albedo, tends to maintain the surface cooling, while the reduced upward longwave flux and the sensible heat flux tend to damp the surface cooling (Table 1).

We also use the general equilibrium feedback assessment method to study the relative contributions of the change in surface incoming shortwave and change in reflected shortwave by surface albedo variation to the biquadrate of surface air temperature in Table 1. Déry and Brown (2007) have shown that the snow-albedo feedback in the Northern Hemisphere is most sensitive in spring. So here we only choose spring monthly data, or the feedback coefficient will be highly underestimated. We also use biquadrate temperature as the dependent variable according to the black body radiation formula. The result shows that the surface incoming shortwave flux change induced by cloud cover change explains 45.78% of total variation, while the reflected shortwave by surface albedo change explains 31.78%. The decrease in surface temperature, in turn, maintains the surface snow cover. The regression of the snow mass increases by 10%. The feedback between snow and the albedo is probably the main cause of the decrease in temperature in the lower and middle troposphere over Central Siberia. An increase in snow cover leads to a greater reflection of shortwave radiation and lowers the surface temperature, which, in turn, maintains the surface snow cover. Cooling of the middle troposphere facilitates the condensation of moisture and cloud formation. The increase in total cloud cover, which leads to a greater reflection of shortwave radiation, and increased snowfall may be secondary factors. The decrease in temperature induces cyclonic circulation anomalies over Central Siberia and therefore enhances the emission of dust over East Asia.

Further, regressions of the dust column mass, dust surface mass, dust emission, column dust transportation flux, and dust sedimentation against the time series of the EOF mode of dust emission were performed, and results are shown in Figure 10 to illustrate the association of these variables with the dust emission over East Asian deserts caused by the feedbacks over Central Siberia. When the spring snow mass and snow cover increase over Central Siberia (Figures 8a and 8c), significant positive spring dust emission regression coefficients occur in the Gobi Desert and reach 100 mg·m^{-2}·day^{-1}, whereas no significant anomalies occur in the Taklimakan Desert. As a result of the increase in the 700-hPa northwesterly wind (Figure 6a) and surface wind (Figure 7b), the column dust transportation flux increases by 0.5 mg·m^{-1}·s^{-1} over both the Taklimakan and Gobi Deserts (Figure 10a). The dust emission from the Taklimakan Desert is not affected by the snow-albedo feedback and the cloud-albedo feedback, but the transport of dust over the desert increases due to the feedbacks. A similar magnitude of significant positive column dust transportation flux anomalies occurs from northern China to the Korean Peninsula, which suggests that the feedbacks have stronger effects on downstream areas with lower dust densities. There are significantly positive dust column mass regression

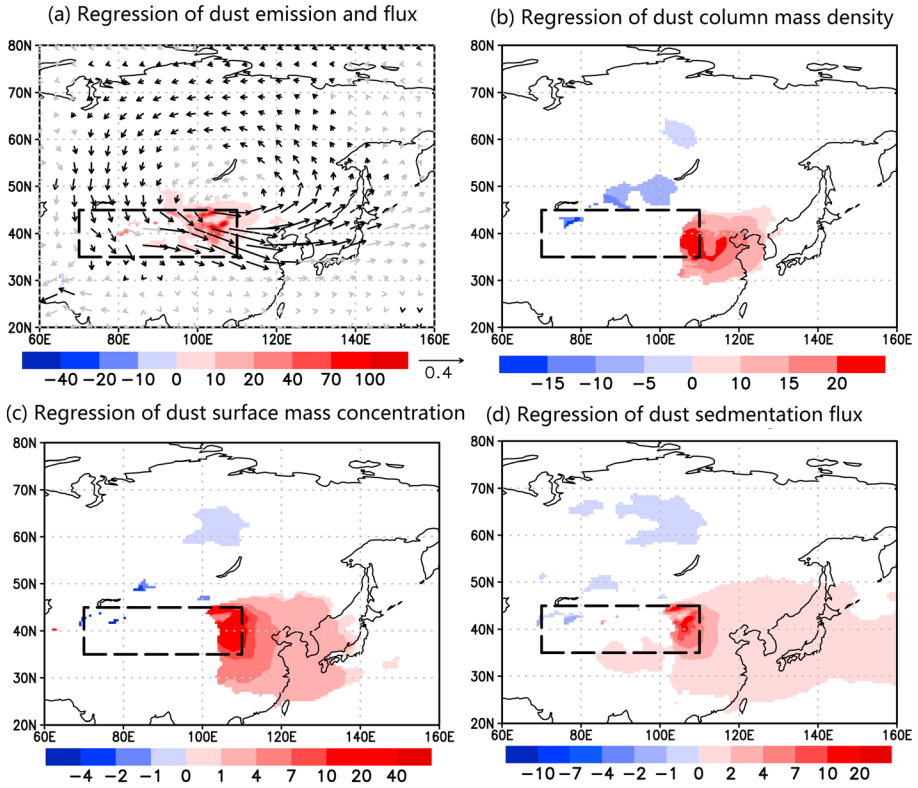

Figure 10. Regressions of spring mean (a) dust flux (vectors, unit: $g \cdot m^{-1} \cdot s^{-1}$) and dust emission flux (colored, unit: $mg \cdot m^{-2} \cdot day^{-1}$), (b) dust column mass density (unit: mg/m^2), (c) dust surface mass concentration ($\mu g/m^3$), and (d) dust sedimentation (unit: $mg \cdot m^{-2} \cdot day^{-1}$) against the time series of the empirical orthogonal function mode of dust emission. Colored areas indicate that regressions pass the significance test at the 95% significance level. Black dashed line boxes indicate the East Asian desert regions.

coefficients over eastern China (105–125°E, 30–45°N; Figure 10b). The regression coefficients in dust surface mass, which is more related to dust storms, are spread comparatively over a wider region of (100–140°E, 25–50° N) where dust surface mass increases by 4 mg/m^3 over northern China. These results imply that a higher DSF over East Asia is associated with more snow cover and snow mass over Central Siberia. The distribution of the dust sedimentation regression coefficients shows the wide range of significant anomalies. The Tibetan Plateau, northern and eastern China, Japan, and even the Western Pacific receive significantly more dust sedimentation. The strengthened northwesterly winds over the source and downstream regions enhance the emission and transportation of dust. The increase in dust column mass and dust sedimentation over the downstream regions leads to more dust storms and therefore increased aerosol-radiation and aerosol-cloud interactions, and increased continental and maritime fertilization, influencing the East Asian climate system. These environmental effects may be more pronounced on the scale of hundreds or thousands of years.

3.3. Relationship Between Spring East Asian Dust Cycle and the Preceding Winter AO

To determine the relationship of interannual variations between the pre-spring large-scale circulation and the spring dust emission in East Asia, the 500-hPa geopotential height in the preceding winter in MERRA2 data set was regressed against the time series of the dominant dust emission EOF mode during 1980 to 2016. The results are shown in Figure 11. In the preceding winter before a spring with high dust emission in East Asia, significant positive 500-hPa geopotential height regression coefficients occur over the Arctic and negative 500-hPa geopotential height regression coefficients occur over midlatitudes in the Atlantic Ocean, Europe, and the Western Pacific (Figure 11a). The pattern of these geopotential regression coefficients resembles the negative phase of AO (Thompson et al.,2000). The correlation between the winter AO index and the time series of the first EOF dust emission mode is −0.56 (Figure 11b). It is possible that the spring

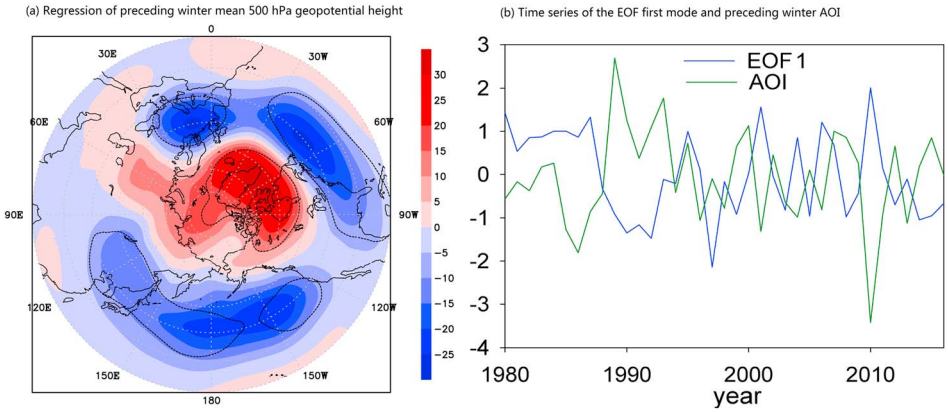

Figure 11. (a) The regression of preceding winter 500-hPa geopotential height (colored, unit: m) against the time series of the first empirical orthogonal function (EOF) mode of spring East Asian dust emission during 1980–2016. Dashed contours highlight areas where regressions pass the significance test at the 95% confidence level. (b) Time series of the first EOF mode of dust emission and year-to-year variation of the preceding winter mean Arctic Oscillation index (AOI) obtained from the National Oceanic and Atmospheric Administration.

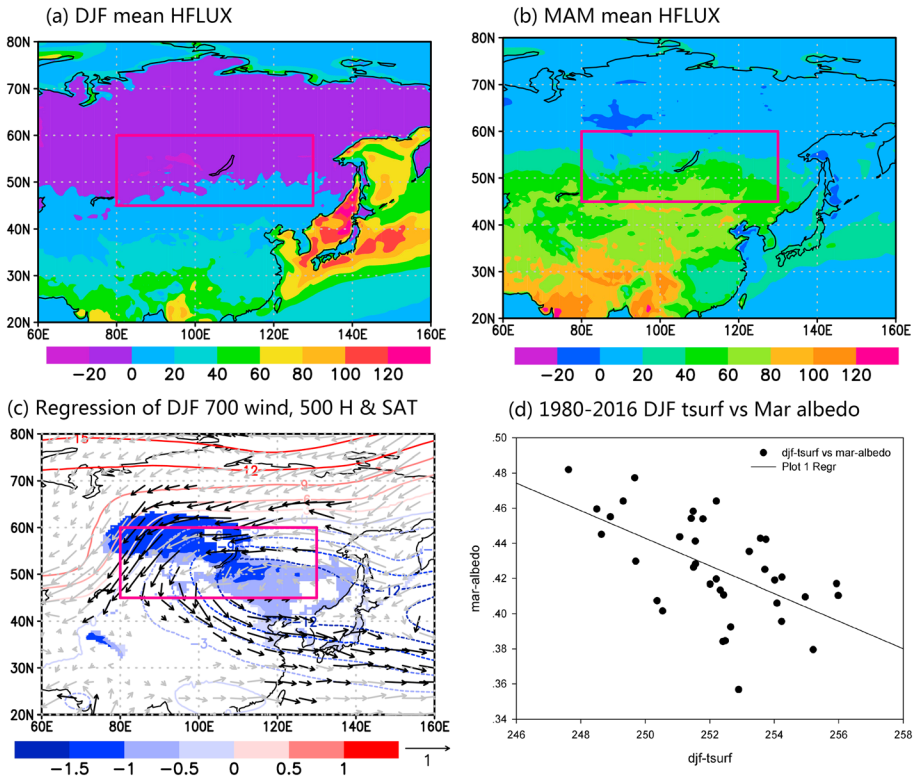

Figure 12. (a) The climatological (1980–2016) mean winter sensible heat flux from turbulence (HFLUX; colored, unit: W/m^2). (b) Same as (a) but for spring (colored, unit: W/m^2). (c) Regression of preceding winter mean 700-hPa wind (vectors, unit: m/s), geopotential height (contour, unit: m), and surface temperature (colored, unit: K) onto the time series of the first empirical orthogonal function mode of spring East Asian dust emission during 1980–2016. Colored area and black vector highlight regressions that pass the significance test at 95% the confidence level. (d) The 1980–2016 year-to-year scatter map of preceding winter surface temperature of land (TSURF; unit: K) and March albedo averaged for Central Siberian (80–130°E, 45–60°N). Red box represents Central Siberia. DJF = December–January–February; MAM = March–April–May; SAT = surface air temperature.

dust cycle in East Asia might be also related to the activities of the AO in spring. However, the correlation between the spring AO index and the time series of the first EOF dust emission mode is only −0.35 and is much weaker than the correlation with the winter AO index, suggesting strong influence of preceding winter AO on dust emission. This is consistent with previous studies that have shown that the winter AO index is significantly correlated with the DSF over East Asia (Mao et al., 2011). AO activity in the preceding winter will not directly influence the spring dust emission but will modify the winter circulation in East Asia and influence land surface processes in Central Siberia in winter. The anomalous land surface conditions can persist into spring, be amplified by positive feedbacks highlighted in previous sections, and eventually initiate the snow-albedo and cloud-albedo feedbacks to influence the spring dust emission over East Asia.

We further analyzed the surface processes on Central Siberia to interpret how land surface signals induced by winter AO persist to spring. The climatological land sensible heat flux from turbulence (Roads & Betts, 2000) in winter over Central Siberia is generally negative (Figure 12a) and turns to positive in spring (Figure 12b). That means, in winter, the surface air heats the land in Central Siberia, whereas the opposite effect occurs in spring. Yeo et al. (2017) showed that cold winds from the Arctic surged into Siberia during the negative phase of AO. So we further regressed the preceding winter circulation and surface temperature of land onto time series of dust emission EOF mode to explain the connection between the winter AO and spring snow-albedo and cloud feedbacks. The preceding winter circulation regression indicates that northeasterly wind anomalies occur over the northern domain, and land surface temperature regression shows that cold anomalies occur in Central Siberia before spring with high dust emission (Figure 12c). Therefore, during the negative phase of AO, cold air from the Arctic cools the land surface in Central Siberia in winter. These negative land surface temperature anomalies in winter increase the surface albedo in the next March (Figure 12d), initiate the positive snow-albedo and cloud-albedo feedbacks in the next spring, and are further amplified by themselves in the next spring.

4. Conclusions

After evaluating the reliability and validity of used data by comparing reanalysis data from the MERRA2 data set with other data from satellites and meteorological stations, we further explored the spatiotemporal characteristics of East Asian dust cycle and the potential factors influencing its interannual variation. The following three conclusions were drawn:

1. The East Asian dust cycle is most active in spring, while the Gobi Desert located on the border of China and Mongolia and the Taklimakan Desert located in the Tarim Basin contribute the most of the dust emission. Although the emission from the Taklimakan Desert is twice as much as that from the Gobi Desert, the main year-to-year variations of the dust cycle in spring are attributed to the Gobi Desert as the dominant dust emission EOF mode suggested. The midlatitude westerlies prevail above 600 hPa over both the deserts in spring. At surface, the Gobi Desert and Taklimakan Desert are controlled by westerly winds and easterly winds, respectively. The dust cycle of East Asia highly depends on the dominant dust emission EOF mode. The dust column mass, the dust surface mass, and the dust deposition over downstream areas from northern China to northwestern Pacific are positively associated with the emission from the Gobi Desert and have little relation to the Taklimakan Desert, because the Taklimakan airborne dust is difficult to escape from the basin.
2. The variation of dust emission in spring over the Gobi Desert is closely related to snow-albedo feedback and cloud-albedo feedback in Central Siberia. An increase in the snow cover extent and snow mass in Central Siberia enhances the reflection of shortwave radiation and cools the land, which, in turn, maintains the changes in snow cover and snow mass. Cloud-albedo feedback associated with increased cloud cover through enhancing the relative humidity induced by cooling in the lower and middle troposphere is another significant process to reflect shortwave radiation. The temperature in the lower and middle troposphere in Central Siberia is reduced by these feedbacks. The cooling in the mid-lower troposphere over Central Siberia facilitates the development of a midlatitude westerly trough, the lowering of the isobaric surface, and the formation of the large-scale anomalous cyclonic circulation in the middle and lower troposphere, with enhancing the temperature gradient between Siberia and China. As a result of thermal wind balance, a few days later the mid-lower tropospheric westerly winds over the East Asia and then the surface westerly winds over the Gobi Desert intensify, finally leading to the increasing of the dust emission and the corresponding East Asian dust cycle.

3. The spring East Asian dust cycle is also modified by the activity of AO in the preceding winter. The correlation coefficient between the winter AO index and time series of the first EOF mode of spring East Asian dust emission during 1980–2016 reaches −0.56, significant at the 99% confidence level. During the negative phase of the winter AO, cold air from the Arctic frequently surges into Central Siberia and cools the regional land surface. Since the land surface of Central Siberia gains sensible heat from the air, the surface temperature significantly decreased during the negative phase of the winter AO. The cold land surface temperature anomalies are maintained to increase the snow mass and surface albedo at the beginning of the next spring. Thus, the snow-albedo and cloud-albedo feedbacks are initiated to maintain or further amplify the surface cooling. It is these feedbacks that modulate the regional atmospheric circulation and eventually the East Asian dust cycle as described above in the second conclusion. On the contrast, East Asian dust is inactive during a spring with a positive AO phase in the preceding winter.

There are some previous studies that found a high correlation between preceding winter AO and spring East Asian dust storms (Gao & Washington, 2010; Gong et al., 2006; Han et al., 2008; Mao et al., 2011), but the physical mechanism is not totally revealed. Some studies have found the spring 925-hPa eddy kinetic energy (Gong et al., 2006) and the spring location and intensity of the 500-hPa westerly jet (Han et al., 2008; Mao et al., 2011) may be the cause of interannual variation of East Asian dust cycle. In this study, we revealed the snow-albedo and cloud feedbacks in spring were the key to how winter AO induced surface signal in Central Siberia was persisted to the following spring and amplified by positive feedbacks in spring. The lead-lag correlation analyses in this study illustrated that the decrease in winter surface temperature on Central Siberia was the starting point to initiate the next spring positive snow-albedo and cloud feedbacks. However, AO is not the only factor that can influence the snow cover and snow mass on Central Siberia. Yeo et al. (2017) found that the spring snow cover was generally a decreasing trend in Central Siberia, which may be an effect of global warming. The snow-albedo feedback may intensify the warming trend on higher latitude to decrease the temperature difference between the north and south of East Asian deserts. The weakening of northwesterly winds related to decrease in meridional temperature gradient over the East Asian deserts might be the cause of the decreasing trend in the DSF over East Asia since the 1980s. These issues need to be further tested in the future by using more data or numerical simulations.

Acknowledgments
The MERRA2 reanalysis data, ERA-Interim data, and DSF data of Chinese meteorological stations were obtained from the Goddard Earth Sciences Data and Information Services Center (https://disc.gsfc.nasa.gov), the European Centre for Medium-Range Weather Forecasts (http://apps.ecmwf.int/datasets), and China Meterological Administration (http://www.nmic.gov.cn/), respectively. This work was jointly supported by the Strategic Priority Research Program of Chinese Academy of Sciences (XDA20070103), the National Key Research and Development Program of China (2016YFA0601904), and the National Natural Science Foundation of China (41690115 and 41572150). B. D. was supported by the U.K. National Centre for Atmospheric Science-Climate (NCAS-Climate) at the University of Reading.

References

Bishop, J. K., Davis, R. E., & Sherman, J. T. (2002). Robotic observations of dust storm enhancement of carbon biomass in the North Pacific. *Science*, *298*(5594), 817–821. https://doi.org/10.1126/science.1074961

Björnsson, H., & Venegas, S. A. (1997). A manual for EOF and SVD analyses of climatic data. *CCGCR Report*, *97*(1), 112–134.

Bristow, C. S., Hudson-Edwards, K. A., & Chappell, A. (2010). Fertilizing the Amazon and equatorial Atlantic with West African dust. *Geophysical Research Letters*, *37*, L14807. https://doi.org/10.1029/2010GL043486

Brown, R., Derksen, C., & Wang, L. (2010). A multi-data set analysis of variability and change in Arctic spring snow cover extent, 1967–2008. *Journal of Geophysical Research*, *115*, D16111. https://doi.org/10.1029/2010JD013975

Brown, R. D. (2000). Northern Hemisphere snow cover variability and change, 1915–97. *Journal of Climate*, *13*(13), 2339–2355. https://doi.org/10.1175/1520-0442(2000)013<2339:NHSCVA>2.0.CO;2

Brown, R. D., & Robinson, D. A. (2011). Northern Hemisphere spring snow cover variability and change over 1922–2010 including an assessment of uncertainty. *The Cryosphere*, *5*(1), 219–229. https://doi.org/10.5194/tc-5-219-2011

Buchard, V., Randles, C. A., da Silva, A. M., Darmenov, A., Colarco, P. R., Govindaraju, R., et al. (2017). The MERRA-2 aerosol reanalysis, 1980 onward. Part II: Evaluation and case studies. *Journal of Climate*, *30*(17), 6851–6872. https://doi.org/10.1175/JCLI-D-16-0613.1

Dee, D. P., Uppala, S. M., Simmons, A. J., Berrisford, P., Poli, P., Kobayashi, S., et al. (2011). The ERA-Interim reanalysis: Configuration and performance of the data assimilation system. *Quarterly Journal of the Royal Meteorological Society*, *137*(656), 553–597. https://doi.org/10.1002/qj.828

Deer, Z. (1984). Synoptic-climatic studies of dust fall in China since historic times. *Science in China Series B-Chemistry, Biological, Agricultural, Medical & Earth Sciences*, *27*(8), 825–836.

Déry, S. J., & Brown, R. D. (2007). Recent Northern Hemisphere snow cover extent trends and implications for the snow-albedo feedback. *Geophysical Research Letters*, *34*, L22504. https://doi.org/10.1029/2007GL031474

Ding, R., Li, J., Wang, S., & Ren, F. (2005). Decadal change of the spring dust storm in northwest China and the associated atmospheric circulation. *Geophysical Research Letters*, *32*, L02808. https://doi.org/10.1029/2004GL021561

Falkowski, P. G., Barber, R. T., & Smetacek, V. (1998). Biogeochemical controls and feedbacks on ocean primary production. *Science*, *281*(5374), 200–206. https://doi.org/10.1126/science.281.5374.200

Gao, H., & Washington, R. (2010). Arctic Oscillation and the interannual variability of dust emissions from the Tarim Basin: A TOMS AI based study. *Climate Dynamics*, *35*(2–3), 511–522. https://doi.org/10.1007/s00382-009-0687-4

Gelaro, R., McCarty, W., Suárez, M. J., Todling, R., Molod, A., Takacs, L., et al. (2017). The modern-era retrospective analysis for research and applications, version 2 (MERRA-2). *Journal of Climate*, *30*(14), 5419–5454. https://doi.org/10.1175/JCLI-D-16-0758.1

Ginoux, P., Chin, M., Tegen, I., Prospero, J. M., Holben, B., Dubovik, O., & Lin, S. J. (2001). Sources and distributions of dust aerosols simulated with the GOCART model. *Journal of Geophysical Research*, *106*(D17), 20,255–20,273. https://doi.org/10.1029/2000JD000053

Gong, D. Y., Mao, R., & Fan, Y. D. (2006). East Asian dust storm and weather disturbance: Possible links to the Arctic Oscillation. *International Journal of Climatology*, *26*(10), 1379–1396. https://doi.org/10.1002/joc.1324

Han, Y., Fang, X., Kang, S., Wang, H., & Kang, F. (2008). Shifts of dust source regions over central Asia and the Tibetan Plateau: Connections with the Arctic Oscillation and the westerly jet. *Atmospheric Environment*, *42*(10), 2358–2368. https://doi.org/10.1016/j.atmosenv.2007.12.025

Huang, J., Wang, T., Wang, W., Li, Z., & Yan, H. (2014). Climate effects of dust aerosols over East Asian arid and semiarid regions. *Journal of Geophysical Research: Atmospheres*, *119*, 11,398–11,416. https://doi.org/10.1002/2014JD021796

Huete, A., Didan, K., Miura, T., Rodriguez, E. P., Gao, X., & Ferreira, L. G. (2002). Overview of the radiometric and biophysical performance of the MODIS vegetation indices. *Remote Sensing of Environment*, *83*(1–2), 195–213. https://doi.org/10.1016/S0034-4257(02)00096-2

Kang, L., Huang, J., Chen, S., & Wang, X. (2016). Long-term trends of dust events over Tibetan Plateau during 1961–2010. *Atmospheric Environment*, *125*, 188–198. https://doi.org/10.1016/j.atmosenv.2015.10.085

Karyampudi, V. M., & Carlson, T. N. (1988). Analysis and numerical simulations of the Saharan air layer and its effect on easterly wave disturbances. *Journal of the Atmospheric Sciences*, *45*(21), 3102–3136. https://doi.org/10.1175/1520-0469(1988)045<3102:AANSOT>2.0.CO;2

Karyampudi, V. M., & Pierce, H. F. (2002). Synoptic-scale influence of the Saharan air layer on tropical cyclogenesis over the eastern Atlantic. *Monthly Weather Review*, *130*(12), 3100–3128. https://doi.org/10.1175/1520-0493(2002)130<3100:SSIOTS>2.0.CO;2

Kawamoto, K. (2008). Effect of precipitation on water cloud properties over China. *Geophysical Research Letters*, *35*, L20811. https://doi.org/10.1029/2008GL035052

Knippertz, P., & Stuut, J. B. W. (2014). Introduction. In *Mineral dust* (pp. 1–14). Dordrecht: Springer.

Levin, Z., Ganor, E., & Gladstein, V. (1996). The effects of desert particles coated with sulfate on rain formation in the eastern Mediterranean. *Journal of Applied Meteorology*, *35*(9), 1511–1523. https://doi.org/10.1175/1520-0450(1996)035<1511:TEODPC>2.0.CO;2

Littmann, T. (1991). Dust storm frequency in Asia: Climatic control and variability. *International Journal of Climatology*, *11*(4), 393–412.

Liu, H., Liu, X., & Dong, B. (2017). Intraseasonal variability of winter precipitation over central Asia and the western Tibetan Plateau from 1979 to 2013 and its relationship with the North Atlantic Oscillation. *Dynamics of Atmospheres and Oceans*, *79*, 31–42. https://doi.org/10.1016/j.dynatmoce.2017.07.001

Liu, X., Yin, Z. Y., Zhang, X., & Yang, X. (2004). Analyses of the spring dust storm frequency of northern China in relation to antecedent and concurrent wind, precipitation, vegetation, and soil moisture conditions. *Journal of Geophysical Research*, *109*, D16210. https://doi.org/10.1029/2004JD004615

Liu, Z., Liu, D., Huang, J., Vaughan, M., Uno, I., Sugimoto, N., et al. (2008). Airborne dust distributions over the Tibetan Plateau and surrounding areas derived from the first year of CALIPSO lidar observations. *Atmospheric Chemistry and Physics*, *8*(16), 5045–5060. https://doi.org/10.5194/acp-8-5045-2008

Liu, Z., Wen, N., & Liu, Y. (2008). On the assessment of nonlocal climate feedback. Part I: The generalized equilibrium feedback assessment. *Journal of Climate*, *21*(1), 134–148. https://doi.org/10.1175/2007JCLI1826.1

Mahowald, N. M., Baker, A. R., Bergametti, G., Brooks, N., Duce, R. A., Jickells, T. D., et al. (2005). Atmospheric global dust cycle and iron inputs to the ocean. *Global Biogeochemical Cycles*, *19*, GB4025. https://doi.org/10.1029/2004GB002402

Manktelow, P. T., Carslaw, K. S., Mann, G. W., & Spracklen, D. V. (2010). The impact of dust on sulfate aerosol, CN and CCN during an East Asian dust storm. *Atmospheric Chemistry and Physics*, *10*(2), 365–382. https://doi.org/10.5194/acp-10-365-2010

Mao, R., Ho, C. H., Shao, Y., Gong, D. Y., & Kim, J. (2011). Influence of Arctic Oscillation on dust activity over northeast Asia. *Atmospheric Environment*, *45*(2), 326–337. https://doi.org/10.1016/j.atmosenv.2010.10.020

Marticorena, B., & Bergametti, G. (1995). Modeling the atmospheric dust cycle: 1. Design of a soil-derived dust emission scheme. *Journal of Geophysical Research*, *100*(D8), 16,415–16,430. https://doi.org/10.1029/95JD00690

Merrill, J., Arnold, E., Leinen, M., & Weaver, C. (1994). Mineralogy of aeolian dust reaching the North Pacific Ocean: 2. Relationship of mineral assemblages to atmospheric transport patterns. *Journal of Geophysical Research*, *99*(D10), 21,025–21,032. https://doi.org/10.1029/94JD01734

Merrill, J. T., Uematsu, M., & Bleck, R. (1989). Meteorological analysis of long range transport of mineral aerosols over the North Pacific. *Journal of Geophysical Research*, *94*(D6), 8584–8598. https://doi.org/10.1029/JD094iD06p08584

Miller, R. L., & Tegen, I. (1998). Climate response to soil dust aerosols. *Journal of Climate*, *11*(12), 3247–3267. https://doi.org/10.1175/1520-0442(1998)011<3247:CRTSDA>2.0.CO;2

Miura, T., Huete, A. R., Yoshioka, H., & Holben, B. N. (2001). An error and sensitivity analysis of atmospheric resistant vegetation indices derived from dark target-based atmospheric correction. *Remote Sensing of Environment*, *78*(3), 284–298. https://doi.org/10.1016/S0034-4257(01)00223-1

Prospero, J. M., Ginoux, P., Torres, O., Nicholson, S. E., & Gill, T. E. (2002). Environmental characterization of global sources of atmospheric soil dust identified with the Nimbus 7 Total Ozone Mapping Spectrometer (TOMS) absorbing aerosol product. *Reviews of Geophysics*, *40*(1), 1002. https://doi.org/10.1029/2000RG000095

Qian, W., & Zhu, Y. (2001). Climate change in China from 1880 to 1998 and its impact on the environmental condition. *Climatic Change*, *50*(4), 419–444. https://doi.org/10.1023/A:1010673212131

Randles, C. A., da Silva, A. M., Buchard, V., Colarco, P. R., Darmenov, A., Govindaraju, R., et al. (2017). The MERRA-2 aerosol reanalysis, 1980 onward. Part I: System description and data assimilation evaluation. *Journal of Climate*, *30*(17), 6823–6850. https://doi.org/10.1175/JCLI-D-16-0609.1

Rea, D. K. (1994). The paleoclimatic record provided by eolian deposition in the deep sea: The geologic history of wind. *Reviews of Geophysics*, *32*(2), 159–195. https://doi.org/10.1029/93RG03257

Rea, D. K., & Hovan, S. A. (1995). Grain size distribution and depositional processes of the mineral component of abyssal sediments: Lessons from the North Pacific. *Paleoceanography*, *10*(2), 251–258. https://doi.org/10.1029/94PA03355

Roads, J., & Betts, A. (2000). NCEP–NCAR and ECMWF reanalysis surface water and energy budgets for the Mississippi River basin. *Journal of Hydrometeorology*, *1*(1), 88–94. https://doi.org/10.1175/1525-7541(2000)001<0088:NNAERS>2.0.CO;2

Sokolik, I. N., & Toon, O. B. (1996). Direct radiative forcing by anthropogenic airborne mineral aerosols. *Nature*, *381*(6584), 681–683. https://doi.org/10.1038/381681a0

Su, L., & Fung, J. C. (2015). Sensitivities of WRF-Chem to dust emission schemes and land surface properties in simulating dust cycles during springtime over East Asia. *Journal of Geophysical Research: Atmospheres*, *120*, 11,215–11,230. https://doi.org/10.1002/2015JD023446

Sun, J., Zhang, M., & Liu, T. (2001). Spatial and temporal characteristics of dust storms in China and its surrounding regions, 1960–1999: Relations to source area and climate. *Journal of Geophysical Research*, *106*(D10), 10,325–10,333. https://doi.org/10.1029/2000JD900665

Sun, Y., Zhuang, G., Wang, Y., Zhao, X., Li, J., Wang, Z., & An, Z. (2005). Chemical composition of dust storms in Beijing and implications for the mixing of mineral aerosol with pollution aerosol on the pathway. *Journal of Geophysical Research*, *110*, D24209. https://doi.org/10.1029/2005JD006054

Tegen, I., Hollrig, P., Chin, M., Fung, I., Jacob, D., & Penner, J. (1997). Contribution of different aerosol species to the global aerosol extinction optical thickness: Estimates from model results. *Journal of Geophysical Research*, *102*(D20), 23,895–23,915. https://doi.org/10.1029/97JD01864

Thompson, D. W., Wallace, J. M., & Hegerl, G. C. (2000). Annular modes in the extratropical circulation. Part II: Trends. *Journal of Climate*, *13*(5), 1018–1036. https://doi.org/10.1175/1520-0442(2000)013<1018:AMITEC>2.0.CO;2

Wang, N., & Zhang, Y. (2015). Connections between the Eurasian teleconnection and concurrent variation of upper-level jets over East Asia. *Advances in Atmospheric Sciences*, *32*(3), 336–348. https://doi.org/10.1007/s00376-014-4088-1

Wang, S., Wang, J., Zhou, Z., & Shang, K. (2005). Regional characteristics of three kinds of dust storm events in China. *Atmospheric Environment*, *39*(3), 509–520. https://doi.org/10.1016/j.atmosenv.2004.09.033

Wang, X., Huang, J., Ji, M., & Higuchi, K. (2008). Variability of East Asia dust events and their long-term trend. *Atmospheric Environment*, *42*(13), 3156–3165. https://doi.org/10.1016/j.atmosenv.2007.07.046

Washington, R., Todd, M., Middleton, N. J., & Goudie, A. S. (2003). Dust-storm source areas determined by the total ozone monitoring spectrometer and surface observations. *Annals of the Association of American Geographers*, *93*(2), 297–313. https://doi.org/10.1111/1467-8306.9302003

Winker, D. M., Hostetler, C. A., Vaughan, M. A., & Omar, A. H. (2006). CALIOP algorithm theoretical basis document, part 1: CALIOP instrument, and algorithms overview. Release, 2, 29.

Winker, D. M., Hunt, W. H., & McGill, M. J. (2007). Initial performance assessment of CALIOP. *Geophysical Research Letters*, *34*, L19803. https://doi.org/10.1029/2007GL030135

Wu, J., Zha, J. L., Zhao, D. M., & Yang, Q. D. (2017). Effects of surface friction and turbulent mixing on long-term changes in the near-surface wind speed over the Eastern China Plain from 1981 to 2010. *Climate Dynamics*, *51*(5-6), 2285–2299. https://doi.org/10.1007/s00382-017-4012-3

Xuan, J., & Sokolik, I. N. (2002). Characterization of sources and emission rates of mineral dust in Northern China. *Atmospheric Environment*, *36*(31), 4863–4876. https://doi.org/10.1016/S1352-2310(02)00585-X

Yeo, S. R., Kim, W., & Kim, K. Y. (2017). Eurasian snow cover variability in relation to warming trend and Arctic Oscillation. *Climate Dynamics*, *48*(1–2), 499–511. https://doi.org/10.1007/s00382-016-3089-4

Yin, Y., & Chen, L. (2007). The effects of heating by transported dust layers on cloud and precipitation: A numerical study. *Atmospheric Chemistry and Physics*, *7*(13), 3497–3505. https://doi.org/10.5194/acp-7-3497-2007

Yu, Y., Notaro, M., Wang, F., Mao, J., Shi, X., & Wei, Y. (2017a). Observed positive vegetation-rainfall feedbacks in the Sahel dominated by a moisture recycling mechanism. *Nature Communications*, *8*(1), 1873. https://doi.org/10.1038/s41467-017-02021-1

Yu, Y., Notaro, M., Wang, F., Mao, J., Shi, X., & Wei, Y. (2017b). Validation of a statistical methodology for extracting vegetation feedbacks: Focus on North African ecosystems in the community earth system model. *Journal of Climate*, *31*(4), 1565–1586. https://doi.org/10.1175/JCLI-D-17-0220.1

Zhang, X. Y., Arimoto, R., & An, Z. S. (1997). Dust emission from Chinese desert sources linked to variations in atmospheric circulation. *Journal of Geophysical Research*, *102*(D23), 28,041–28,047. https://doi.org/10.1029/97JD02300

Zhang, X. Y., Gong, S. L., Zhao, T. L., Arimoto, R., Wang, Y. Q., & Zhou, Z. J. (2003). Sources of Asian dust and role of climate change versus desertification in Asian dust emission. *Geophysical Research Letters*, *30*(24), 2272. https://doi.org/10.1029/2003GL018206